Effect of structure on porous gas-diffusion electrodes for phosphoric acid fuel cells

D.S. Chan and C.C. Wan
Department of Chemical Engineering, National Tsing-Hua University, 30043 Hsin-Cu (Taiwan)

(Received October 29, 1993; accepted December 31, 1993)

Abstract

This investigation is concerned with the variation of structure in the catalyst layer for porous gas-diffusion electrodes. The pore-size distribution and the total pore volume of the electrode are measured by a mercury penetration method. A model that accounts for this incomplete wetting electrode is solved by an orthogonal collocation method and matched with experimental observations. The numerical solution indicates that the effectiveness factor drops noticeably under high current density when the agglomerate radius is greater than 40 μm. When the agglomerate radius is smaller than 1.2 μm, however, the effect of ionic transport becomes important. The maximum reaction rate occurs at carbon-paper/catalyst-layer interface when the effective conductivity of the electrolyte is larger than that of the solid phase. If the effective conductivity of the electrolyte is smaller, then the maximum reaction rate occurs at the electrode/electrolyte interface.

Introduction

The performance of a porous gas-diffusion electrode is much affected by the intrinsic activity of the platinum catalyst and the wettability of the electrode. It is generally recognized that the major concern in developing an efficient electrode is to reduce the path of oxygen diffusion to the active sites of the platinum in the catalyst layer by either changing the platinum content [1–3] or improving the wettability of the electrode [4–14]. As it is not feasible to increase the platinum content because of cost considerations, improvement in wettability seems to be more practical. It has also been observed that the acid absorption of the electrode decreases as the polytetrafluoroethylene (PTFE) content in the catalyst layer or the baking temperature of the electrode increases [13, 14]. These results indicate that a very low or high wettability of the catalyst layer leads to poor performance. Giordano *et al.* [14] have recommended that the PTFE content in the catalyst layer should be about 30 to 50 wt.% and the baking temperature to be 330 to 350 °C. Kunz *et al.* [15] found double Tafel slopes when oxygen diffusion was significantly hindered in a porous gas-diffusion electrode.

The electrode's wettability must be optimized to provide good ionic and electric conductivity, reactant transport, and platinum utilization. Many theoretical models have been developed to simulate the performance of porous gas-diffusion electrodes used in phosphoric acid fuel cells (PAFCs) [16–19]. Few papers have been published, however, with respect to the influence of structure on the diffusion and reaction within the electrode. In this work, a study has been made of the change of structure by using different PTFE contents, and of its effect on the agglomerate radius. The

SSDI 0378-7753(94)01898-6

agglomerate radius is used to calculate the effectiveness factor, solid and electrolyte potential profiles, and reaction-rate distribution within the electrode structure.

Experimental

Test electrodes, each with dual carbon paper and catalyst layers, were prepared according to the procedure described previously [20]. The test cell and the experimental methods for obtaining the oxygen reduction response and the acid absorption have also been reported [20].

The pore volume filled with electrolyte in the catalyst layer was calculated by dividing the weight difference before and after the acid absorption experiment by the specific gravity of phosphoric acid. The pore-size distribution of the electrode was measured by the mercury penetration method. The electronic conductivity in the catalyst layer was determined by a collinear four-probe method. The true density was obtained with a helium pycnometer.

Model development

Giner and Hunter [16] have proposed a flooded agglomerate model to describe the performance characteristics of a fuel cell electrode. In this model, the porous catalyst layer is assumed to be a number of cylinders in parallel. The void between the cylinders is filled with gas. A cylinder in which catalyst particles and electrolyte are homogeneously dispersed is illustrated schematically in Fig. 1. The cylinder with agglomerate length δ and agglomerate radius r_0 is perpendicular to the surface of the carbon paper. The performance of porous gas-diffusion electrodes used in PAFCs is controlled primarily by the rate of oxygen reduction on the platinum catalyst. The mass balance equation for the dissolved oxygen in the cylinders is given by:

$$\bar{D}_l \frac{1}{r} \frac{\partial}{\partial r} \left[r \frac{\partial C_l(z, r)}{\partial r} \right] = \frac{ai(z, r)}{nF} \tag{1}$$

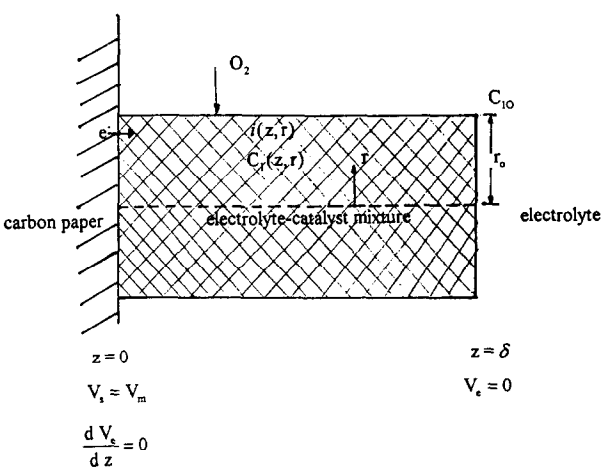

Fig. 1. Schematic representation of agglomerate model [16].

where $\bar{D}_l$ is the effective diffusivity of dissolved oxygen, a the surface-volume ratio, n the number of electrons involved in the electrode reaction; $C_l(z, r)$ is the dissolved oxygen concentration, $i(z, r)$ is the local current density, and F is the Faraday constant. The local current density in the cylinder can then be expressed by:

$$i(z, r) = i_0 \frac{C_l(z, r)}{C_{lO}} \exp\left(- \frac{E(z) - E_{OCV}}{T_a} \right) \tag{2}$$

where i_0 is exchange current density; $E(z)$ the electrode potential, E_{OCV} the open-circuit potential, T_a the Tafel slope, which is approximately 0.09 V/decade [15] in this case. C_{lO} is the concentration of dissolved oxygen at the gas-cylinder interface. The equilibrium between the oxygen in the gas phase and at the cylinder interface is governed by Henry's law. Therefore:

$$C_{lO} = \frac{Y_l P_T}{HRT} \tag{3}$$

where Y_l is the mole fraction of oxygen in the gas phase, P_T the total pressure, and H, Henry's law constant, which is 55 for 85% phosphoric acid at 180 °C [21]. Combining eqns. (1) and (2) gives:

$$\bar{D}_l \frac{1}{r} \frac{\partial}{\partial r} \left[r \frac{\partial C_l(z, r)}{\partial r} \right] = \frac{a i_0}{nF} \frac{C_l(z, r)}{C_{lO}} \exp\left(- \frac{E(z) - E_{OCV}}{T_a} \right) \tag{4}$$

This is basically the Butler–Volmer equation with the anodic term deleted since the reaction is controlled mainly by the oxygen reduction. Equation (4) is similar to that of Giner and Hunter [16], except that the Tafel slope and cathodic term have also been taken into consideration in this study. The two boundary conditions for eqn. (4) are:

$$\frac{\partial C_l}{\partial r} = 0 \quad \text{at } r = 0 \tag{5}$$

$$C_l(r_0, z) = C_{lO} \quad \text{at } r = r_0 \tag{6}$$

Potential distribution within the agglomerate cylinder

The electrode potential can be written as:

$$E(z) = \phi_s(z) - \phi_e(z) \tag{7}$$

where $\phi_s(z)$ is the solid potential and $\phi_e(z)$ the electrolyte potential.

The potential gradient in the electrolyte can be expressed by Ohm's law:

$$\frac{d\phi_e(z)}{dz} = \frac{I_i(z)}{\pi r_0^2 \bar{k}_e} \tag{8}$$

where I_i is the ionic current, and $\bar{k}_e$ is the effective conductivity of electrolyte in the agglomerate. The current generated can be expressed as:

$$\frac{dI_i}{dz} = 2\pi a \int_0^{r_0} ir \, dr \tag{9}$$

Differentiating eqn. (8) and eliminating dI_i/dz by eqn. (9) yields:

$$\frac{d^2\phi_e}{dz^2} = \frac{2a}{r_0^2\bar{k}_e}\int_0^{r_0} ir\,dr \tag{10}$$

Equation (10) has been developed by Kunz [22] for a molten carbonate cathode.

The measured electrode potential (E_m) is the potential difference between the potential in the solid phase at $z=0$ and the potential in the electrolyte at $z=\delta$, namely:

$$E_m = \phi_s|_{z=0} - \phi_e|_{z=\delta} \tag{11}$$

where $\phi_s|_{z=0}$ is the potential of the solid phase at $z=0$, and $\phi_e|_{z=\delta}$ is the potential of the electrolyte at $z=\delta$. Setting $\phi_e|_{z=\delta}=0$, gives:

$$E_m = \phi_s|_{z=0} \tag{12}$$

The two boundary conditions for eqn. (10) are:

$$\phi_e|_{z=\delta}=0 \tag{13}$$

$$\left.\frac{d\phi_e}{dz}\right|_{z=0} = 0 \tag{14}$$

The solid potential gradient is related to the electronic current as follows:

$$\frac{d\phi_s(z)}{dz} = \frac{I_e(z)}{\pi r_0^2\bar{k}_s} \tag{15}$$

where I_e is the electronic current and $\bar{k}_s$ is the effective conductivity of the solid phase in the agglomerate.

The overall current, I_t, for the entire cylinder can be evaluated at $z=\delta$, which is:

$$I_t = \pi r_0^2\bar{k}_e\left.\frac{d\phi_e}{dz}\right|_{z=\delta} \tag{16}$$

The sum of the ionic current and electronic current is constant at each point along the cylinder and must be equal to the total current [22]. Mathematically, this means that:

$$I_t = I_i + I_e \text{ at any } z \tag{17}$$

$$I_i = 0,\ I_e = I_t \text{ at } z=0,\ I_i = I_t,\ I_e = 0 \text{ at } z=\delta \tag{18}$$

Therefore, the electronic current is given by:

$$I_e = I_t - I_i \tag{19}$$

Substitution eqns. (8) and (16) into eqn. (15) yields:

$$\frac{d\phi_s}{dz} = \frac{\bar{k}_e}{\bar{k}_s}\left(\left.\frac{d\phi_e}{dz}\right|_{z=\delta} - \left.\frac{d\phi_e}{dz}\right|_{z=z}\right) \tag{20}$$

The boundary condition for eqn. (20) is:

$$\phi_s = E_m \text{ at } z=0 \tag{21}$$

Equation (20) coupled with eqn. (10) can then be solved and the potential profiles (ϕ_e and ϕ_s) can be used for the calculation of the apparent current density, I_a, as

represented by:

$$I_a = N\pi r_0^2 \bar{k}_e \left.\frac{d\phi_e}{dz}\right|_{z=\delta} \tag{22}$$

where N is the number of agglomerate cylinders per unit area of electrode.

Calculation of agglomerate properties

Kunz *et al.* [22] developed a method to calculate the size of agglomerates in molten carbonate fuel cell electrodes. They indicated that the agglomerate radius was increased by increasing the electrolyte quantity in the catalyst layer. The method can also be applied to PAFC electrodes [20]. When the applied pressure is greater than the liquid pressure, PV work (PdV) is done to increase the vapour-liquid interfacial free energy (σdA). The relation between the PdV and the σdA is

$$PdV = -\sigma dA \tag{23}$$

where P is the differential pressure between the gas pressure (P_G) and liquid pressure (P_L), V the gas volume, A the vapour-liquid interfacial area, σ the surface tension of electrolyte. The differential pressure in the gas-filled pores is balanced by the surface tension of the electrolyte in the pores. The relation between the differential pressure ($P_G - P_L$) and surface tension can be written as [22]:

$$P_G - P_L = \frac{2\sigma}{r} \tag{24}$$

where r is the pore radius obtained from the pore-size distribution graph by mercury penetration method.

Combination of eqn. (23) and eqn. (24) yields:

$$dA = \frac{2dV}{r} \tag{25}$$

Integrating eqn. (25) yields:

$$A = \int_{V_f}^{V_t} \frac{2}{r}\, dV \tag{26}$$

where V_t is the total pore volume of the catalyst layer and V_f the pore volume wetted by electrolyte in the catalyst layer. If electrolyte and catalyst can be considered a homogeneous continuum [16, 22], the agglomerate radius, the vapour-liquid interfacial area and the pore volume wetted by electrolyte are related by:

$$\frac{A}{V_f} = \frac{2N\pi r_0 \tau_e \delta}{N\pi r_0^2 \tau_e \delta} \tag{27}$$

where N is the number of agglomerate cylinders, τ_e the agglomerate tortuosity, and δ the thickness of catalyst layer. Equation (27) can be further simplified, i.e.:

$$\frac{A}{V_f} = \frac{2}{r_0} \tag{28}$$

Eliminating A from eqns. (26) and (28), gives the following relation between r_0 and V:

$$r_0 = \frac{V_f}{\int_{V_f}^{V_t} \frac{1}{r} dV} \tag{29}$$

The agglomerate radius can be estimated according to eqn. (29). The effective conductivity of the electrolyte, the effective conductivity of the solid phase, and the effective diffusivity of the dissolved oxygen in the agglomerate can be expressed as follows [22]:

$$\bar{k}_e = \frac{\theta}{\tau_e} k_e \tag{30}$$

$$\bar{k}_s = \frac{1-\theta}{\tau_s} k_s \tag{31}$$

and,

$$\bar{D}_l = \frac{\theta}{\tau_e} D_l \tag{32}$$

where θ is agglomerate porosity, k_e the electrolyte conductivity which is 0.60 Ω^{-1} cm^{-1} [23] for 98% phosphoric acid at 180 °C, τ_e the ionic tortuosity, k_s the electronic conductivity which can be measured by collinear four-probe method, and τ_s is the agglomerate tortuosity, which is taken as unity.

The agglomerate porosity can be expressed as [22]:

$$\theta = \frac{V_f}{V_f + V_s} \tag{33}$$

where V_s is the solid volume. The number of agglomerate cylinders can also be obtained by:

$$N = \frac{d_a(V_f + V_s)}{\pi r_0^2 \tau_e} \tag{34}$$

where d_a is the apparent density which can be computed by the following relation:

$$V_t = \frac{1}{d_a} - \frac{1}{d_s} \tag{35}$$

where d_s is the true density of electrode as reported in Table 1.

TABLE 1

Properties of test electrodes

	PTFE content (wt.%)			
	20	30	40	50
Total pore volume (cm^3 g^{-1})	1.7026	1.4451	1.1020	0.9830
Agglomerate radius (μm)	40.0	4.8	1.2	0.32
Electronic conductivity (Ω^{-1} cm^{-1})	0.532	0.464	0.470	0.402
True density (g cm^{-3})	2.235	2.216	2.152	2.253

The effectiveness factor is to ascertain whether the reaction is limited by pore diffusion. An effectiveness factor can be defined as [24]:

$$E_f = \frac{\text{actual reaction rate with pore}}{\text{rate if not slowed by pore diffusion}} \tag{36}$$

Using the definition for the agglomerate cylinder, E_f can be written as follows:

$$E_f = \frac{\int_0^{r_0} kC_l r\,dr}{\int_0^{r_0} kC_{lO} r\,dr} = \frac{2}{r_0^2}\int_0^{r_0} \frac{C_l}{C_{lO}} r\,dr \tag{37}$$

where k is the rate constant for a first-order reaction. For the oxygen reaction in the agglomerate, k can be written as:

$$k(z) = \frac{ai_0}{nF}\exp\left(-\frac{E(z)-E_{OCV}}{T_a}\right) \tag{38}$$

Equation (4) can be integrated to give:

$$\int_0^{r_0} \bar{D}_l \frac{\partial}{\partial r}\left[r\frac{\partial C_l}{\partial r}\right] dr = \int_0^{r_0} \frac{ai_0}{nF}\frac{C_l}{C_{lO}}\exp\left(-\frac{E(z)-E_{OCV}}{T_a}\right) r\,dr \tag{39}$$

From eqns. (39) and (38), we can obtain

$$\frac{\bar{D}_l}{k} r \frac{\partial C_l}{\partial r}\bigg|_{r=0}^{r=r_0} = \int_0^{r_0} \frac{C_l}{C_{lO}} r\,dr \tag{40}$$

Equation (40) can be simplified to:

$$\frac{\bar{D}_l}{k} r_0 \frac{\partial C_l}{\partial r}\bigg|_{r=r_0} = \int_0^{r_0} \frac{C_l}{C_{lO}} r\,dr \tag{41}$$

Combining eqns. (37) and (41) gives:

$$E_f(z) = \frac{2\bar{D}_l}{r_0 kC_{lO}} \frac{\partial C_l}{\partial r}\bigg|_{r=r_0} \tag{42}$$

Equation (42) can be used to calculate the effectiveness factor, which is a function of the electrode position. The differential balance over an incremental length Δz produces the following relation between the ionic current and the local reaction rate, R_l:

$$\pi r_0^2 I_i|_{z=z} + nF\pi r_0^2 \Delta z R_l = \pi r_0^2 I_i|_{z=z+\Delta z} \tag{43}$$

Division by $\pi r_0^2 \Delta z$, and as Δz approaches zero, eqn. (43) becomes:

$$R_l = \frac{1}{nF\pi r_0^2}\frac{dI_i}{dz} \tag{44}$$

Eliminating dI_i/dz by eqn. (9) and i by eqn. (2), yields:

$$R_l = \frac{2a}{nFr_0^2} \int_0^{r_0} \frac{i_0 C_l}{C_{lO}} \exp\left(- \frac{E(z) - E_{OCV}}{T_a} \right) r \, dr \tag{45}$$

Equation (45) can be rearranged to give:

$$R_l = \frac{2ai_0}{nFr_0^2} \exp\left(- \frac{E(z) - E_{OCV}}{T_a} \right) \int_0^{r_0} \frac{C_l}{C_{lO}} r \, dr \tag{46}$$

On substituting eqn. (41) into eqn. (46) to eliminate the $\int_0^{r_0} C_l/C_{lO} r \, dr$ factor, the local reaction rate is obtained as:

$$R_l = \frac{2\bar{D}_l}{r_0} \frac{\partial C_l}{\partial r}\bigg|_{r=r_0} \tag{47}$$

Equation (47) can be used to calculate the sum of the local reaction rates, R_s, i.e.:

$$R_s = \frac{1}{\delta} \int_0^{\delta} R_l(z) \, dz \tag{48}$$

The local relative reaction rate can then be calculated as follows:

$$R_r(z) = \frac{R_l(z)}{R_s} \tag{49}$$

Results and discussion

The porous gas-diffusion electrode contains PTFE as a binder. This material can give mechanical strength and hydrophobicity to the catalyst layer for oxygen diffusion. The pores are formed among the carbon supports. The effect of the PTFE content on the porosity distribution is shown in Fig. 2. The total pore volume can be calculated by mercury penetration; it is the cumulative intrusion volume at the maximum diameter. The relation between the total pore volume and the PTFE content is shown in Table 1. It can be seen that the total pore volume is decreased when the PTFE content is increased. This behaviour occurs since the pores are occupied by additional PTFE.

The incremental intrusion volume versus pore diameter is plotted in Fig. 3. These electrodes all have a trimodal pore-size distribution. In Fig. 3, three regions can be distinguished, namely: macropores (>10 μm), micropores (from 0.1 to 10 μm), and fine pores (<0.01 μm).

The agglomerate radius calculated according to eqn. (29) versus the percentage of the pore volume filled with electrolyte is presented in Fig. 4. The agglomerate radius is increased by increasing the percentage of the pore volume filled with electrolyte. The result, due to an increase in the quantity of electrolyte, has been pointed out by Kunz *et al.* [22]. The effect of PTFE content on the agglomerate radius is also shown in Fig. 4. At a constant percentage of the pore volume filled with electrolyte, the agglomerate radius is greater as the PTFE content is decreased. For example, the agglomerate is greater for 20 wt.% than for 30 wt.% PTFE. This trend occurs because the total pore volume is decreased when the PTFE content is increased. The effect of PTFE content on the agglomerate radius from measured data is shown in

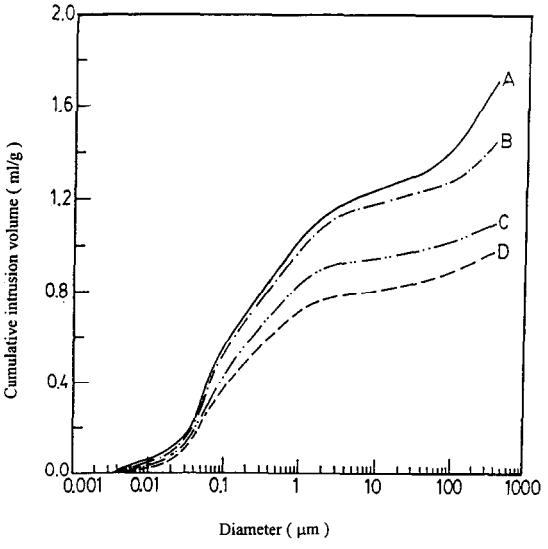

Fig. 2. Porosity spectra of electrodes with different PTFE contents and baked at 340 °C. PTFE content (wt.%): (A) 20; (B) 30; (C) 40, and (D) 50.

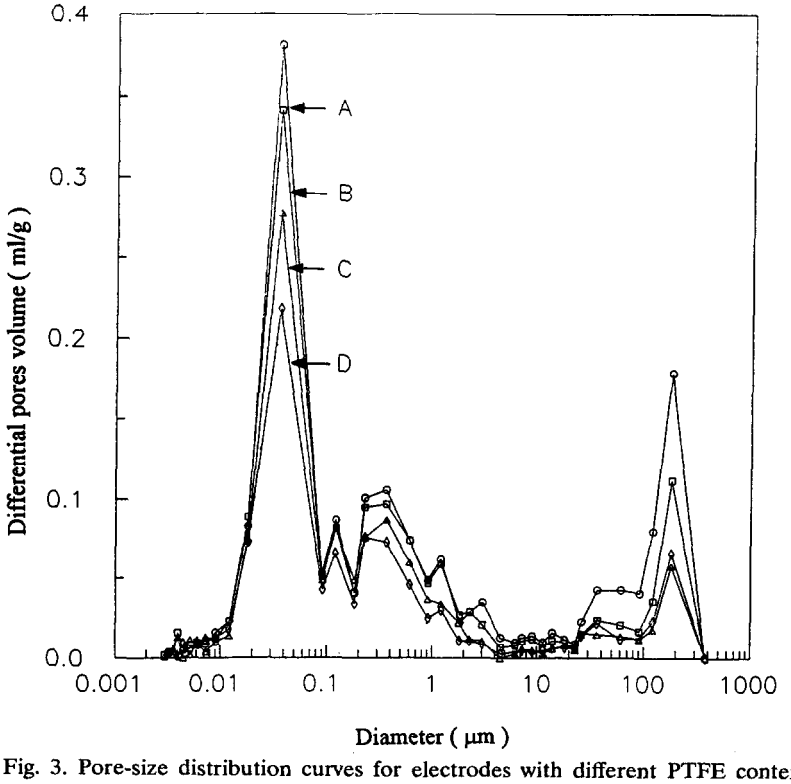

Fig. 3. Pore-size distribution curves for electrodes with different PTFE contents and baked at 340 °C. PTFE content (wt.%): (A) 20; (B) 30; (C) 40, and (D) 50.

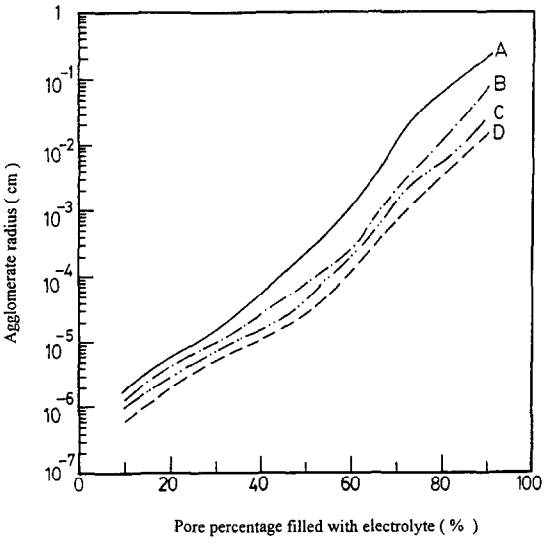

Fig. 4. Agglomerate radius of electrode vs. percentage of volume filled by electrolyte. PTFE content (wt.%): (A) 20; (B) 30; (C) 40, and (D) 50.

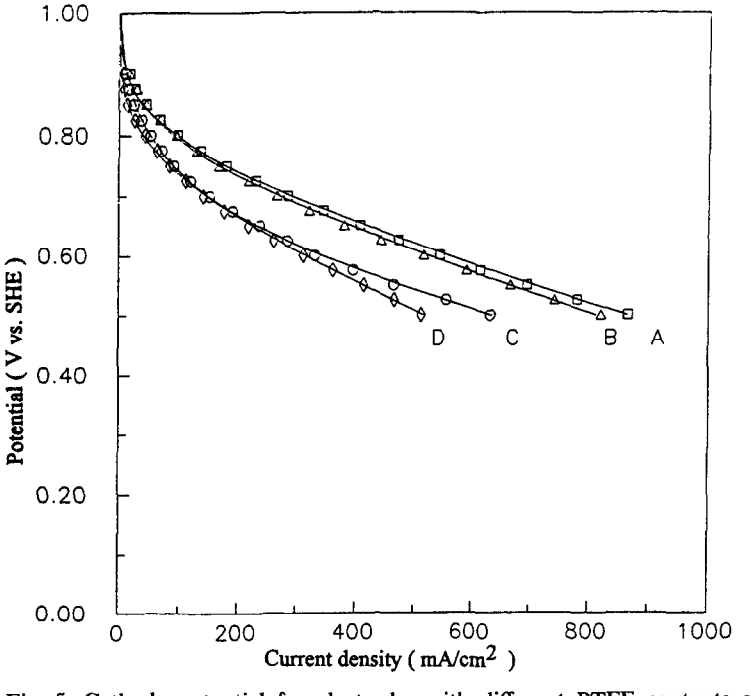

Fig. 5. Cathode potential for electrodes with different PTFE contents and baked at 340 °C. Actual data points are indicated by symbols and model calculations are indicated by continuous curves. PTFE content (wt.%): (A) 30; (B) 40; (C) 20, and (D) 50.

Table 1. The behaviour indicates that the agglomerate radius decreases with increasing PTFE content.

The results from the model's prediction and experimental data for four different test electrodes are given in Fig. 5. The curves calculated by the model agree well with those obtained by experiment. The agglomerate radius used in the model is related to the ionic tortuosity as follows: $\tau_e = 0.849 - 0.135 \ln r_0$, where the agglomerate radius is between 40 and 0.32 μm and the ionic tortuosity is between 1.61 and 2.27. As mentioned above, the electrode performance data were taken under potentiostatic conditions and the current density was measured at the desired electrode potential. The theoretical prediction in Fig. 5 was made by solving eqns. (10) and (20) using the orthogonal collocation method [25]. At least 20 collocation points were used to improve the accuracy of the numerical solutions. The model can be used for the investigation of the effectiveness factor, local relative reaction rate and potential profiles, which will be discussed in the next section.

Effectiveness factor distribution within electrode structure

To design a heterogeneous reactor, it is common to employ the concept of an effectiveness factor to determine whether the reaction is limited by pore diffusion [26]. This concept can be applied to design a porous gas-diffusion electrode where the platinum catalyst is coated on the surface of the carbon support. The effectiveness factor would be unity if there is no diffusional limitation within the agglomerate. The results of the four electrodes examined here are shown in Figs. 6 to 9, respectively. The result from Fig. 6 indicates that the effectiveness factor drops markedly when the potential is <0.7 V (curves C and D). When the electrode has a large agglomerate radius (40 μm), the electrode suffers voltage loss from the mass-transport resistance of dissolved oxygen; the effectiveness factor distribution is quite uniform along each position at different potentials. The performance of the electrode with a large agglomerate radius (40 μm) is controlled by pore diffusion. The result from Fig. 7, however, shows that the effectiveness factor strongly depends on the electrode's location at potentials <0.7 V (curves C and D). The electrode with a 4.8 μm agglomerate radius is controlled by pore diffusion when the potential is <0.7 V. When the agglomerate radius is <1.2 μm, the effectiveness factor (Figs. 8 and 9) is almost unity at all positions and various potentials. Those electrodes with an agglomerate radius smaller than 1.2 μm are regarded to have no limitation to dissolved oxygen. A high PTFE content reduces the agglomerate radius so that the voltage loss due to diffusion of dissolved oxygen is decreased.

Solid and electrolyte potential profiles within the electrode structure

The electronic conductivities in the catalyst layer were measured, the results are given in Table 1. It can be seen that the electronic conductivity decreases in response to the increased PTFE content. This is reasonable since PTFE is an electronic insulator. The effective conductivity of the electrolyte and the effective conductivity of the solid phase in the agglomerate were then calculated according to eqns. (30) and (31), respectively. The data are recorded in Table 2.

Potential profiles of test electrodes with 20 to 50 wt.% PTFE are given in Figs. 10 to 13, respectively. These results show the potential as a function of electrode position, where $z=1$ represents the dimensionless position located at the electrode/electrolyte interface and $z=0$ represents the position at the carbon-paper/catalyst-layer interface. If the agglomerate radius is >4.8 μm, the smallest potential difference between the solid phase and the electrolyte is at the carbon-paper/catalyst-layer interface,

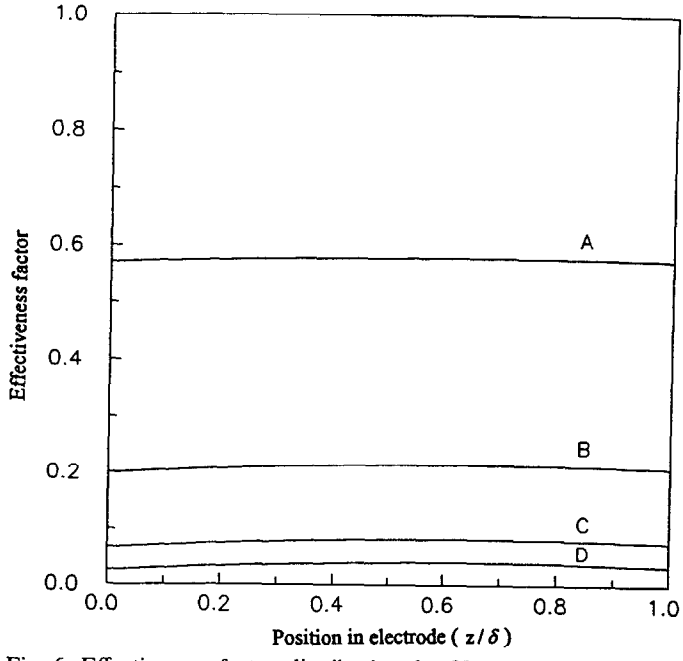

Fig. 6. Effectiveness factor distribution for 20 wt.% PTFE electrode with 40 μm agglomerate radius. Potential (V): (A) 0.9; (B) 0.8; (C) 0.7, and (D) 0.6.

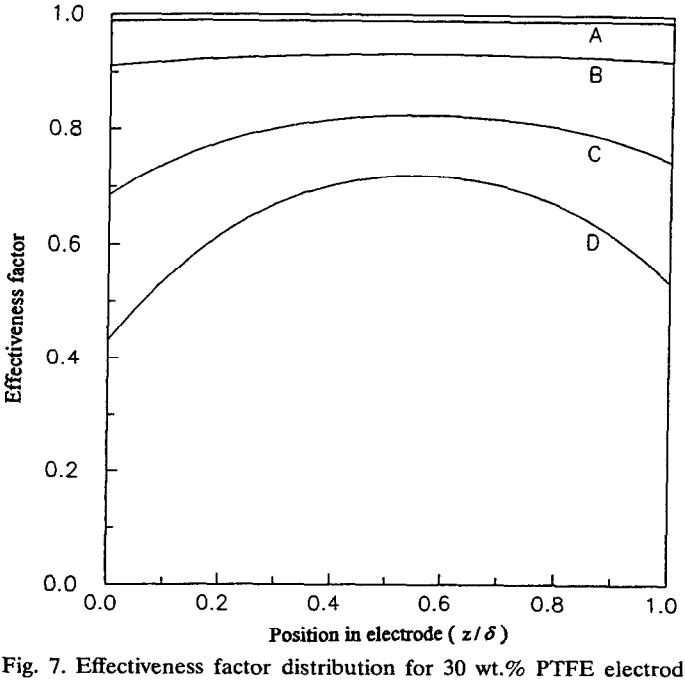

Fig. 7. Effectiveness factor distribution for 30 wt.% PTFE electrode with 4.8 μm agglomerate radius. Potential (V): (A) 0.9; (B) 0.8; (C) 0.7, and (D) 0.6.

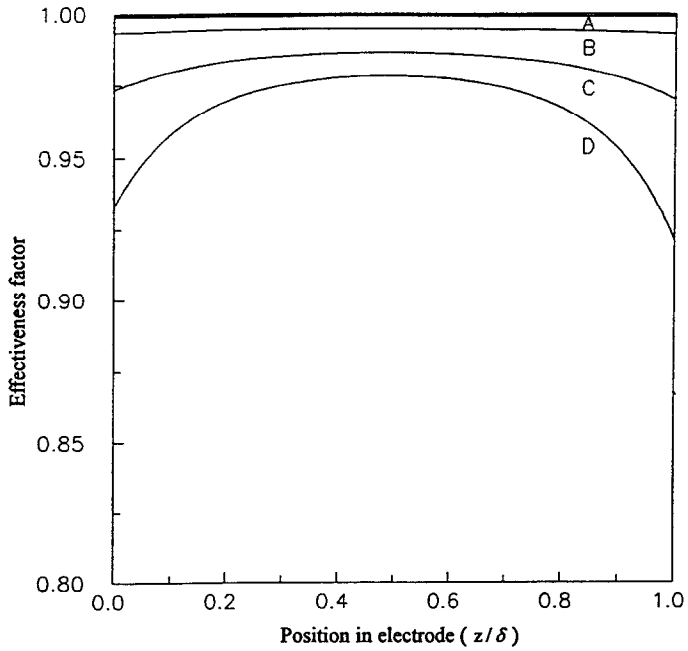

Fig. 8. Effectiveness factor distribution for 40 wt.% PTFE electrode with 1.2 μm agglomerate radius. Potential (V): (A) 0.9; (B) 0.8; (C) 0.7, and (D) 0.6.

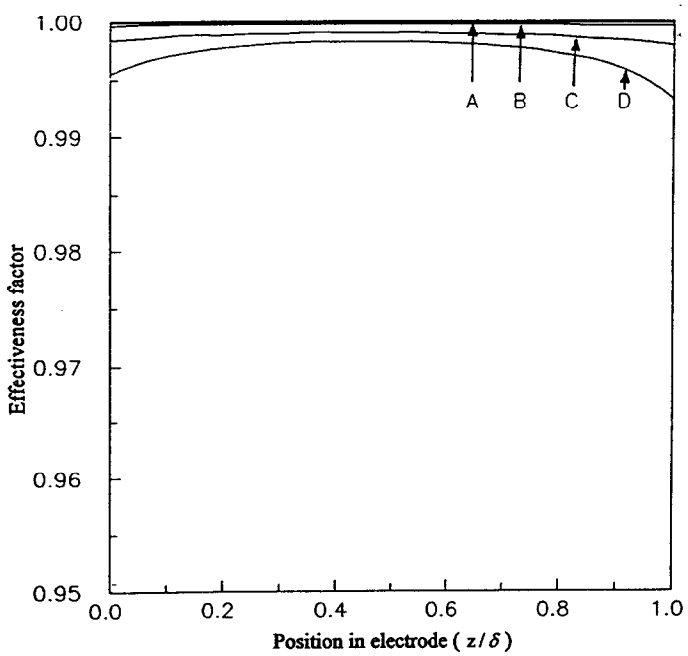

Fig. 9. Effectiveness factor distribution for 50 wt.% PTFE electrode with 0.32 μm agglomerate radius. Potential (V): (A) 0.9; (B) 0.8; (C) 0.7, and (D) 0.6.

TABLE 2

Electric conductivities of test electrodes

	PTFE content (wt.%)			
	20	30	40	50
Effective conductivity of electrolyte, $\bar{k}_e$ (Ω^{-1} cm^{-1})	0.2651	0.2159	0.1708	0.1398
Effective conductivity of solid phase, $\bar{k}_s$ (Ω^{-1} cm^{-1})	0.1530	0.1554	0.1928	0.1885
Ratio of $\bar{k}_e$ and $\bar{k}_s$	1.7327	1.3893	0.8859	0.7416

as shown in Figs. 10 and 12. The smallest potential difference is directly related to the maximum reaction rate. In these cases, the effective conductivity of the solid phase is lower than the effective conductivity of the electrolyte. When the agglomerate radius is <1.2 μm, the smallest potential difference between the solid phase and the electrolyte is at the electrode/electrolyte interface, as shown in Figs. 12 and 13. In these cases, the effective conductivity of the solid phase is larger than that of the electrolyte. Therefore, the local reaction rate is controlled by the effective conductivity of both the electrolyte and the solid phase.

Relative reaction-rate distribution within electrode structure

Yang *et al.* [19] simulated the performance of a porous gas-diffusion electrode in a system in which the effective conductivity of the solid phase is much greater than that of the electrolyte. They pointed out that the maximum reaction rate was at an electrode/electrolyte interface for electrodes with a PTFE content between 30 to 60 wt.%. These data are listed in Table 3. The ratios of $\bar{k}_e$ and $\bar{k}_s$ are all very small in this system. The maximum reaction rate hence occurred at the electrode/electrolyte interface, since the effective conductivity of the electrolyte was smaller than that of the solid phase. In the system presented here, the electronic conductivity was measured in the catalyst layer by a collinear four-probe method and eqns. (30) and (31) were used to calculate the effective conductivity of both the electrolyte and the solid phase. Figures 14 to 17 show the relative reaction rate of oxygen reduction with different PTFE contents that range from 20 to 50 wt.%. These curves show the relative reaction rate as a function of electrode position. The reaction rate appears to be quite uniform when the electrode is controlled at a high potential, e.g., curve D of Fig. 14. When the potential is below 0.7 V, the reaction-rate distribution becomes non-uniform (curves A and B). If the ratio of $\bar{k}_e$ and $\bar{k}_s$ is larger than 1, the maximum reaction rate is located at the carbon-paper/catalyst-layer interface. For instance, Fig. 14 or 15 show that the maximum reaction rate of the electrode with 20 or 30 wt.% PTFE occurs at the carbon-paper/catalyst-layer interface ($z=0$). When the ratio of $\bar{k}_e$ and $\bar{k}_s$ is smaller than 1, the maximum reaction rate occurs at the electrode/electrolyte interface. For example, Figs. 16 or 17 show that the maximum reaction rate is at the electrode/electrolyte interface ($z=1$) for electrodes with 40 or 50 wt.% PTFE. Hence, whether the maximum reaction rate occurs at the carbon-paper/catalyst-layer interface or at the electrode/electrolyte interface depends on the ratio of $\bar{k}_e$ and $\bar{k}_s$. Newman *et al.* [27] reported that the uniformity of the reaction rate within an electrode was determined

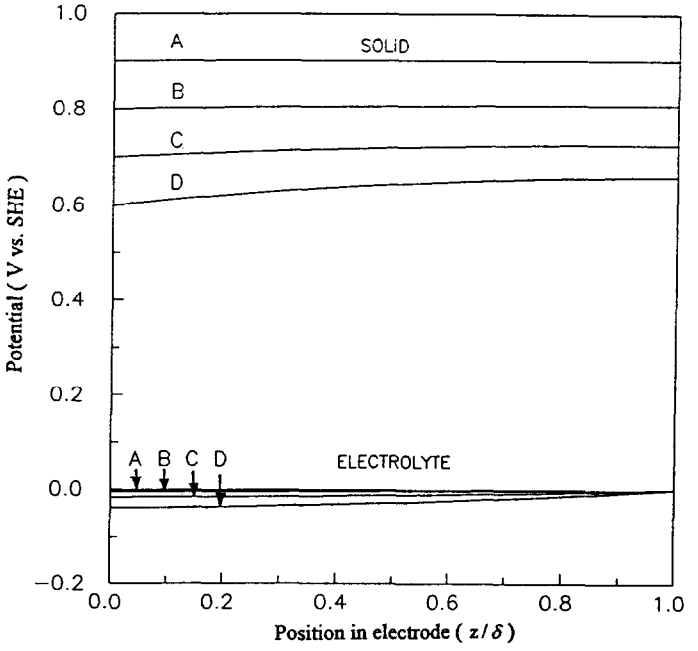

Fig. 10. Potential profile for 20 wt.% PTFE electrode with 40 μm agglomerate radius. Potential (V): (A) 0.9; (B) 0.8; (C) 0.7, and (D) 0.6.

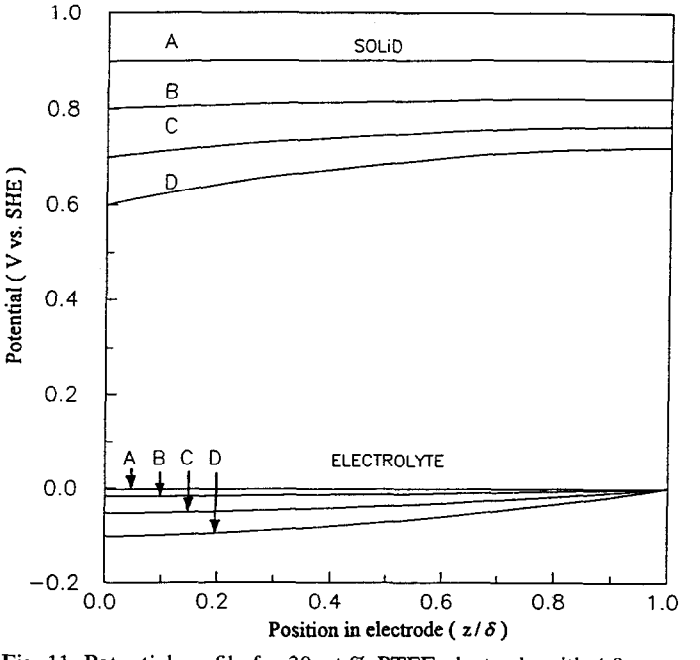

Fig. 11. Potential profile for 30 wt.% PTFE electrode with 4.8 μm agglomerate radius. Potential (V): (A) 0.9; (B) 0.8; (C) 0.7, and (D) 0.6.

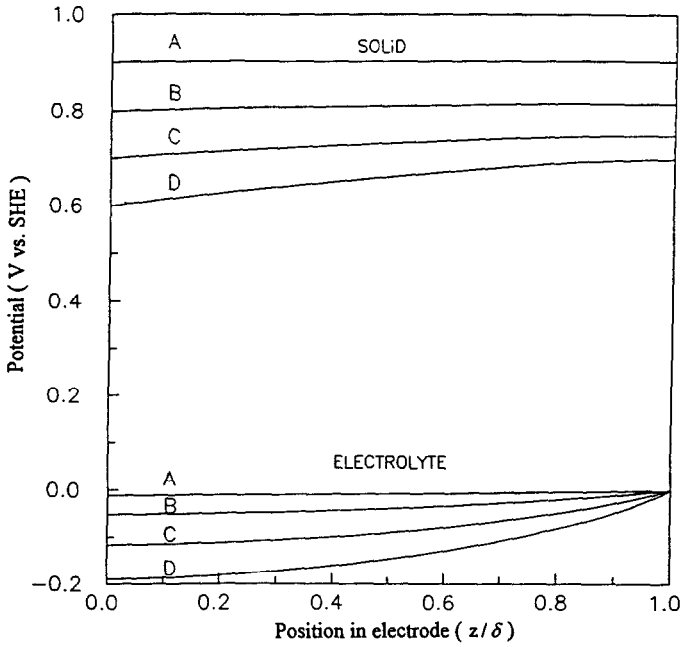

Fig. 12. Potential profile for 40 wt.% PTFE electrode with 1.2 μm agglomerate radius. Potential (V): (A) 0.9; (B) 0.8; (C) 0.7, and (D) 0.6.

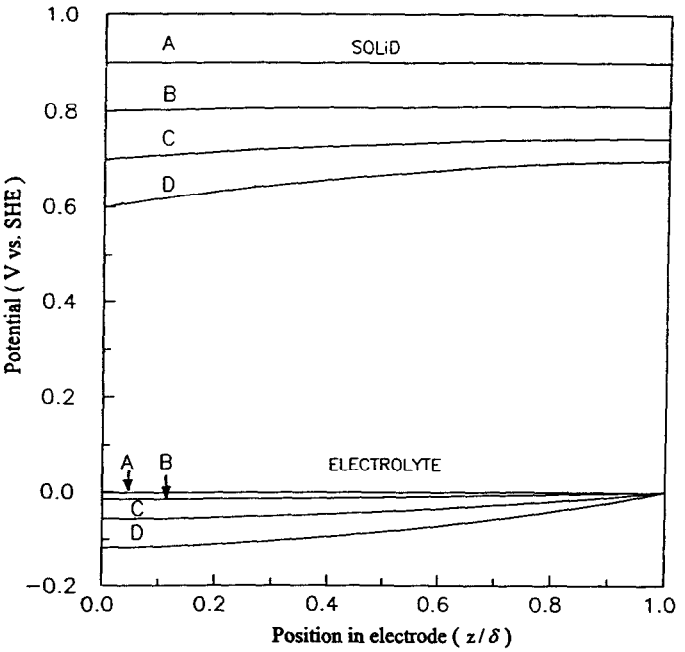

Fig. 13. Potential profile for 50 wt.% PTFE electrode with 0.32 μm agglomerate radius. Potential (V): (A) 0.9; (B) 0.8; (C) 0.7, and (D) 0.6.

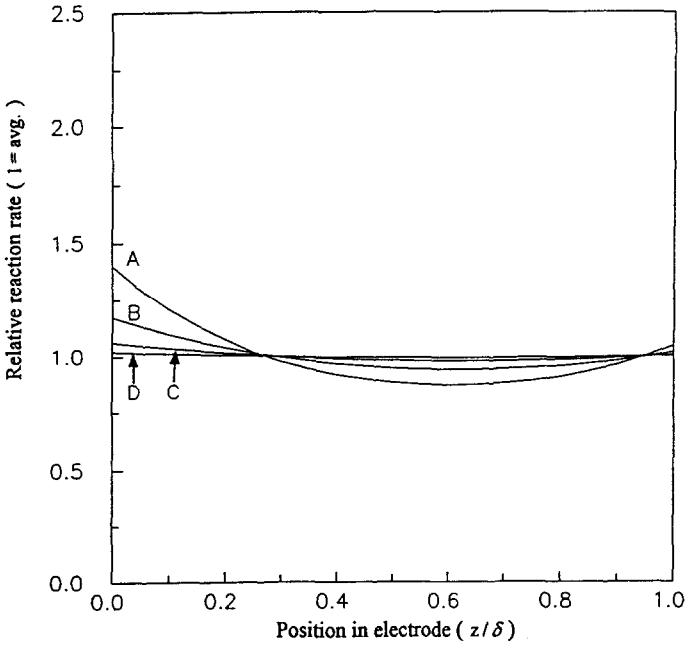

Fig. 14. Local relative rate distribution for 20 wt.% PTFE electrode with 40 μm agglomerate radius. Potential (V): (A) 0.6; (B) 0.7; (C) 0.8, and (D) 0.9.

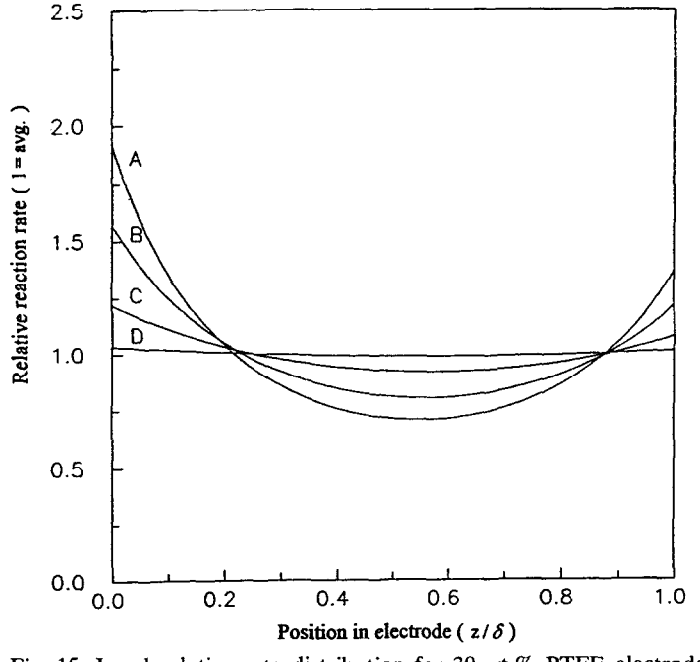

Fig. 15. Local relative rate distribution for 30 wt.% PTFE electrode with 4.8 μm agglomerate radius. Potential (V): (A) 0.6; (B) 0.7; (C) 0.8, and (D) 0.9.

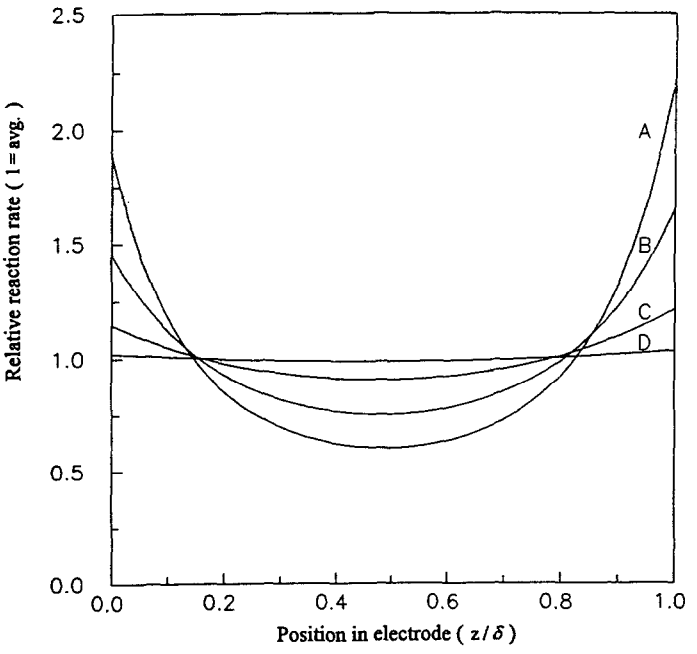

Fig. 16. Local relative rate distribution for 40 wt.% PTFE electrode with 1.2 μm agglomerate radius. Potential (V): (A) 0.6; (B) 0.7; (C) 0.8, and (D) 0.9.

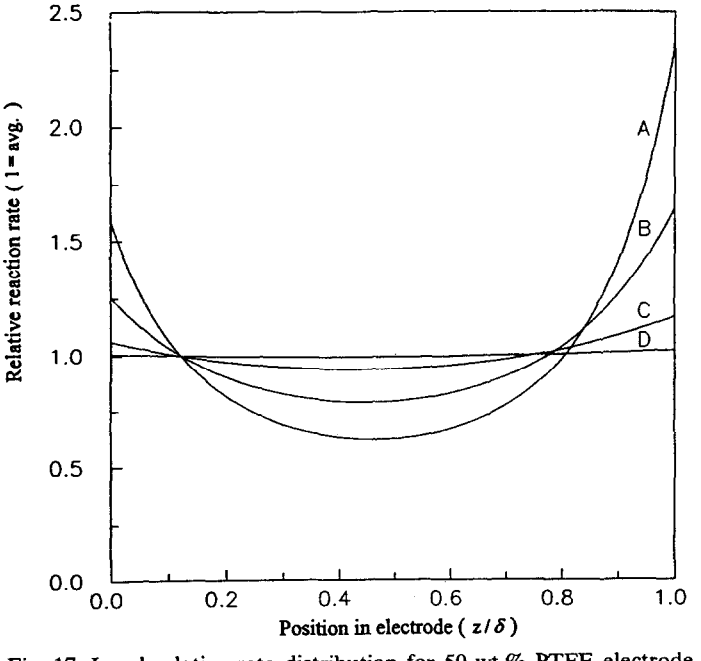

Fig. 17. Local relative rate distribution for 50 wt.% PTFE electrode with 0.32 μm agglomerate radius. Potential (V): (A) 0.6; (B) 0.7; (C) 0.8, and (D) 0.9.

TABLE 3

Electric conductivities of test electrodes [19]

	PTFE content (wt.%)			
	30	40	50	60
Effective conductivity of electrolyte, $\bar{k}_e$ (Ω^{-1} cm^{-1})	0.05656	0.03619	0.03052	0.01923
Effective conductivity of solid phase, $\bar{k}_s$ (Ω^{-1} cm^{-1})	0.9950	0.8598	0.8860	0.8032
Ratio of $\bar{k}_e$ and $\bar{k}_s$	0.0568	0.0421	0.0344	0.0239

by the ratio of the effective conductivities of the electrolyte and the solid phase. They also pointed out that the ratio of $\bar{k}_e$ and $\bar{k}_s$ serves to shift the reaction from one end of the electrode to the other. Their theoretical analysis is consistent with the experimental data presented here.

Conclusions

In a three-phase reaction system, pores with optimal wettability must be formed for satisfactory performance. The agglomerate radius is smaller than 1.2 μm when pores are filled with only a small amount of electrolyte in order to reduce limitations by pore diffusion. The electrolyte quantity can be adjusted by a change in the PTFE content in the catalyst layer. The agglomerate radius can be reduced by increasing the PTFE content so that the voltage loss due to diffusional resistance of dissolved oxygen can be decreased. Using electrodes with an agglomerate radius smaller than 1.2 μm, the effective conductivity of electrolyte is influenced by the reduced amount of electrolyte. The size of the agglomerate cylinder can affect not only the diffusion of the reactant in the catalyst layer, but also the performance of the electrode. The size of the agglomerate cylinder must be controlled by changing the PTFE content. The maximum reaction rate occurs towards the carbon-paper/catalyst-layer interface when $\bar{k}_e$ is larger than $\bar{k}_s$. If $\bar{k}_e$ is smaller than $\bar{k}_s$, the maximum reaction rate occurs nearer to the electrode/electrolyte interface.

Acknowledgements

This study is supported by the Energy Commission of the Ministry of Economic Affairs of Republic of Taiwan through its fuel cell project No. 38k2100. The authors also acknowledge the assistance of the Energy and Resources Laboratories, ITRI.

List of symbols

a	specific interfacial area, cm^{-1}
A	vapour–liquid interfacial area, cm^2
C_l, $C_l(z, r)$	dissolved oxygen concentration at a point (z, r), mol cm^{-3}

C_{lO}	solubility of oxygen, mol cm^{-3}
d_a	apparent density of the electrode, g cm^{-3}
d_s	true density of the electrode, g cm^{-3}
D_l	diffusion coefficient of oxygen, cm^2 s^{-1}
$\bar{D}_l$	effective diffusion coefficient of oxygen in the agglomerate, cm^2 s^{-1}
$E(z)$	electrode potential, V
E_m	measured electrode potential, V
E_{OCV}	open-circuit potential, V
E_f	effectiveness factor of agglomerates as a function of electrode
F	Faraday constant
H	Henry's law constant for oxygen
i, $i(z, r)$	local real current density, A cm^{-2}
i_0	real exchange current density, A cm^{-2}
I_a	apparent current density, A cm^{-2}
I_0	modified Bessel function of order zero
I_1	modified Bessel function of order one
I_i	ionic current, A
I_e	electronic current, A
k	rate constant for a first-order reaction, s^{-1}
k_e	electrolyte conductivity, Ω^{-1} cm^{-1}
$\bar{k}_e$	effective conductivity of electrolyte in the agglomerate, Ω^{-1} cm^{-1}
k_s	electronic conductivity, Ω^{-1} cm^{-1}
$\bar{k}_s$	effective conductivity of solid phase in the agglomerate, Ω^{-1} cm^{-1}
n	number of electrons involved in the electrode reaction
N	number of agglomerate cylinders per unit area of electrode
P	differential pressure between the gas pressure and liquid pressure, atm
P_G	gas pressure, atm
P_L	liquid pressure, atm
P_T	total pressure, atm
r	radial coordinate in the agglomerate cylinder and pore radius, cm
r_0	radius of the agglomerate cylinder, cm
R	gas constant, 82.05 atm cm^3 mol^{-1} K^{-1}
R_l	local relative reaction rate, mol s^{-1} cm^{-3}
R_r, $R_r(z)$	local relative reaction rate, mol s^{-1} cm^{-3}
R_s	sum of local reaction rate, mol^{-1} s^{-1} cm^{-3}
T	absolute temperature, K
T_a	Tafel slope, V
V	volume of gas in the electrode, cm^3
V_f	pores volume wetted by electrolyte in the catalyst layer, cm^3
V_s	solid volume of electrode, cm^3
V_t	total pores volume of catalyst layer, cm^3
Y_l	mole fraction of oxygen in the gas phase
z	axial coordinate in the agglomerate, cm

Greek letters

$\phi(z)$	modified Thiele modulus for z-variation
$\phi_s(z)$	solid potential in the agglomerate, V
$\phi_e(z)$	electrolyte potential, V
δ	length of agglomerate, cm
θ	agglomerate porosity

τ_e	ionic tortuosity
τ_s	agglomerate tortuosity
σ	surface tension of electrolyte, dyne cm^{-1}

References

1 H.R. Kunz and G.A. Gruver, *Electrochim. Acta, 23* (1978) 219.
2 W.M. Vogel and J.T. Lundquist, *J. Electrochem. Soc., 117* (1970) 1512.
3 T. Maoka, *Electrochim. Acta, 33* (1988) 371.
4 S. Motoo, M. Watanabe and N. Furuya, *J. Electroanal. Chem., 160* (1984) 351.
5 M. Watanabe, M. Tomikawa and S. Motoo, *J. Electroanal. Chem., 182* (1985) 193.
6 M. Watanabe, M. Tomikawa and S. Motoo, *J. Electroanal. Chem., 195* (1985) 81.
7 M. Watanabe, K. Makita, H. Usami and S. Motoo, *J. Electroanal. Chem., 197* (1986) 195.
8 J. Giner, J.M. Parry, S. Smith and M. Turchan, *J. Electrochem. Soc., 116* (1969) 1692.
9 W.M. Vogel and K.A. Klinedinst, *Electrochim. Acta, 22* (1977) 1385.
10 B.V. Tilak, R.S. Yeo and S. Srinivasan, in J.O'M. Bockris, B.E. Conway, E. Yeager and R.E. White (eds.), *Comprehensive Treaties Electrochemistry,* Vol. 3, Plenum, New York, 1981, p. 39.
11 Yu.A. Chizmadzhev and Yu.G. Chirkov, in E.B. Yeager, J.O'M. Bockris, B.E. Conway and S. Sarangapani (eds.), *Comprehensive Treaties in Electrochemistry,* Vol. 6, Plenum, New York, 1983, p. 317.
12 T. Maoka, *Electrochim. Acta, 33* (1988) 379.
13 T. Mori, J. Imahashi, T. Kamo, K. Tamura and Y. Hishinuma, *J. Electrochem. Soc., 133* (1986) 896.
14 N. Giordano, E. Passalacqua, V. Recupero, M. Vivaldi, E.J. Taylor and G. Wilemski, *Electrochim. Acta, 35* (1990) 1411.
15 H.R. Kunz and G.A. Gruver, *J. Electrochem. Soc., 122* (1975) 1279.
16 J. Giner and C. Hunter, *J. Electrochem. Soc., 116* (1969) 1124.
17 R.P. Iczkowski and M.B. Cutlip, *J. Electrochem. Soc., 127* (1980) 1433.
18 P. Bjornbom, *Electrochim. Acta, 32* (1987) 115.
19 S.C. Yang, M.B. Cutlip and P. Stonehart, *Electrochim. Acta, 35* (1990) 869.
20 D.S. Chan and C.C. Wan, *J. Power Sources, 50* (1994) 163.
21 K. Klinedinst, J.A.S. Bett, J. Macdonard and P. Stonehart, *J. Electroanal. Chem., 57* (1974) 281.
22 H.R. Kunz, L.J. Bregoli and S.T. Szymanski, *J. Electrochem. Soc., 131* (1984) 2815.
23 D.-T. Chin and H.H. Chang, *J. Appl. Electrochem., 19* (1989) 95.
24 O. Levenspiel, *Chemical Reaction Engineering,* Wiley, New York, 1972.
25 J. Villadsen, M. Michelsen, *Solution to Differential Equation Models by Polynomial Approximation,* Prentice-Hall, Englewood Cliffs, NJ, 1978.
26 C.N. Satterfield, *Mass Transfer in Heterogeneous Catalysis,* Massachusetts Institute of Technology, 1970.
27 J. Newman and W. Tiedemann, *J. Am. Inst. Chem. Eng., 21* (1975) 25.